Available online at www.sciencedirect.com
SCIENCE DIRECT
International Journal of Mass Spectrometry 249–250 (2006) 279–288
International Journal of Mass Spectrometry
www.elsevier.com/locate/ijms

Electron transfer and bond-forming reactions following collisions of SF^{2+} with Ar

Paul W. Burnside, Stephen D. Price *

Chemistry Department, University College London, 20 Gordon Street, London WC1H 0AJ, UK

Received 26 October 2005; accepted 16 December 2005
Available online 23 January 2006

Abstract

Collisions between SF^{2+} and Ar have been investigated using time-of-flight mass spectrometry over a collision energy range of 2.6–6.2 eV in the centre-of-mass frame. The formation of SF^+, S^+ and Ar^+ in single electron transfer reactions has been detected and the cross-sections, in arbitrary units, for forming these species have been evaluated. This electron transfer reactivity has been rationalized by Landau–Zener calculations. The reactivity in this collision system also involves an unusual bond-forming reaction which generates ArS^{2+}. Quantum chemical calculations of the relevant energetics show that the lowest lying singlet and triplet states of ArS^{2+} are bound and are energetically accessible to this collision system at the above collision energies. This energetics analysis also shows that electron transfer in the exit channel between the separating ArS^{2+} and F atom is likely to be inefficient, explaining why we detect the observed products and not $ArS^+ + F^+$.

Keywords: Dication; Electron transfer; Bond-forming

1. Introduction

The investigation of the bimolecular reactivity of small molecular doubly charged ions (dications) has been the focus of an increasing number of experimental initiatives in recent years [1–27] but our understanding of the chemical reactions of these species is still quite restricted. Due to the proximity of the pair of like charges, many electronic states of small molecular dications are unstable, fragmenting to form a pair of monocations [28,29]. However, many molecular dications possess at least one metastable electronic state that lives for a microsecond or more. These metastable states exist due to a barrier to charge-separating dissociation, which can confer on the dication a lifetime of the order of seconds [30].

The bimolecular reactivity of molecular dications has been recently reviewed [4,9,31,32], and the observed reactions can be broadly divided into three classes: (i) electron transfer, (ii) collision-induced fragmentation and (iii) bond-formation. Single electron transfer (SET) processes usually give rise to the most intense product ion signals following collisions between small molecular dications and neutral species. These SET processes may be dissociative or non-dissociative, as exemplified by two reactions of CF_3^{2+} [3]:

$$CF_3^{2+} + Xe \rightarrow CF_2^+ + F + Xe^+ \quad (1)$$

$$CF_3^{2+} + O_2 \rightarrow CF_3^+ + O_2^+ \quad (2)$$

At low collision energies, SET reactions are usually well described by the reaction window model [2,4,31], derived from Landau–Zener theory [33,34]. This model pictures the SET reaction as occurring at the intersection of a reactant potential and a product potential, the so-called curve-crossing. For a dication-neutral collision system the reactant potential is dominated at pertinent interspecies separations by attractive polarization forces. In contrast, the product potential is dominated by the Coulomb repulsion between the product monocations (Fig. 1). Landau–Zener theory defines the probability δ of remaining on one of these diabatic potential energy curves as the system passes through this curve-crossing. In the course of a collision, the system will pass through the intersection twice, but for a successful electron transfer reaction to take place the collision system must only change potential surfaces

* Corresponding author. Tel.: +44 20 7679 4650; fax: +44 20 7679 7463.
E-mail address: S.D.Price@ucl.ac.uk (S.D. Price).

1387-3806/$ – see front matter © 2005 Elsevier B.V. All rights reserved.
doi:10.1016/j.ijms.2005.12.015

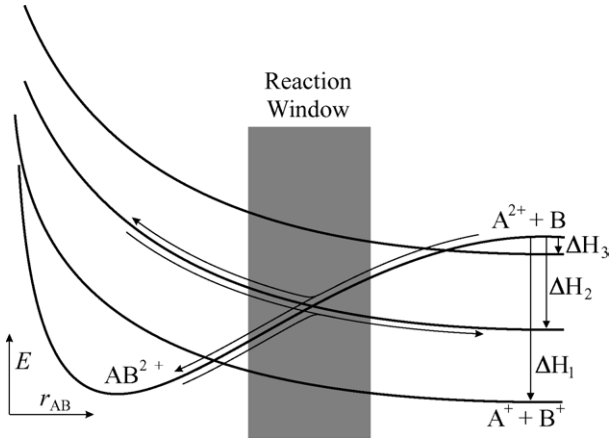

Fig. 1. Schematic potential energy curves showing the reactant potential, for a dication A^{2+} encountering a neutral collision partner B, which is crossed by the potential curves of three electronic states of $A^+ + B^+$. The lowest energy product state, corresponding to a reaction with exothermicity ΔH_1, intersects the reactant curve outside the reaction window where $\delta \approx 0$. The third product state (with exothermicity ΔH_3) also intersects the reactant curve outside the reaction window, where $\delta \approx 1$. At both the above intersections the SET cross-section is predicted to be low. However, the first excited electronic state of $A^+ + B^+$ (with exothermicity ΔH_2) intersects the dication curve within the reaction window, where $\delta \approx 1/2$, and will be significantly populated in an SET reaction. The trajectories show that for SET to occur, the system may switch potentials on either its first or its second pass through the intersection.

once (Fig. 1). Thus, the probability P for SET occurring is:

$$P = \delta(1-\delta) + (1-\delta)\delta = 2\delta(1-\delta) \quad (3)$$

The methodology by which we calculate δ is discussed later, but clearly δ will be close to unity at large crossing radii, because of the weak coupling of the potentials, and decrease as the interspecies separation of the curve-crossing decreases. When the curve-crossing is at small interspecies separations, and the coupling between the two potentials is significant, δ tends to zero. In both of these limits P is approximately zero. However, in the intermediate coupling regime, P reaches a maximum when $\delta = 0.5$. Consequently, SET cross-sections become significant at intermediate values of the crossing radius r_c, in what is termed the 'reaction window', typically between 2 Å and 6 Å. For the prototypical potentials described above, and illustrated in Fig. 1, curve-crossings in the reaction window arise for SET processes with exothermicities between 2 eV and 6 eV.

Double electron transfer processes can also occur following dication-neutral collisions, but at low collision energies such processes are rare and their mechanisms are generally less well understood than SET processes. Most examples of double electron transfer reactions involve the noble gases [35]:

$$^{22}Ne^{2+} + {}^{20}Ne \rightarrow {}^{22}Ne + {}^{20}Ne^{2+} \quad (4)$$

Collision-induced processes are also often observed following dication-neutral collisions [1,4,31,36]. Here the energy supplied by the collision results in the excitation and consequent fragmentation of the parent dication. In these reactions, the double charge may remain localised (5), or separate by the formation of a pair of monocations (6) [3,37]:

$$SF_4^{2+} + CO \rightarrow SF_3^{2+} + F + CO \quad (5)$$

$$CS_2^{2+} + Ar \rightarrow CS^+ + S^+ + Ar \quad (6)$$

Bond-forming reactions of small molecular dications are markedly less common than SET reactions following dication-neutral interactions, but the number observed experimentally is growing steadily. The first reported example of a bond-forming reaction between a small molecular dication and a neutral molecule involved O_2^{2+} [38]:

$$O_2^{2+} + NO \rightarrow NO_2^+ + O^+ \quad (7)$$

Subsequent experiments have observed bond-formation following the collisions of rare gas dications and a variety of small molecular dications with neutral species [3,4,6–8,10,11,14–19,21,24,25,39–41]. The vast majority of these bond-forming reactions produce a pair of singly charged product ions, sometimes accompanied by additional neutral species. However, in recent years the first bond-forming reaction of a non-metallic atomic dication to yield a molecular dication was observed [7]:

$$Ar^{2+} + N_2 \rightarrow ArN^{2+} + N \quad (8)$$

The argon dication also undergoes similar bond-forming reactions with CO and O_2 [6,18]:

$$Ar^{2+} + CO \rightarrow ArC^{2+} + O \quad (9)$$

$$Ar^{2+} + O_2 \rightarrow ArO^{2+} + O \quad (10)$$

Furthermore, considering reaction (10), if the dipositive charge is on the reacting CO molecule and not the argon atom, the same products still result [11]:

$$CO^{2+} + Ar \rightarrow ArC^{2+} + O \quad (11)$$

To date, reaction (11) is the only reported observation of a bond-forming reaction in the gas phase involving small molecular dications as both reactant and product. This paper reports an investigation of the reactivity following collisions of SF^{2+} with Ar. These experiments show that these collisions result in both a bond-forming reaction, which forms ArS^{2+}, and two SET reactions. To rationalize this reactivity we also present a series of ab initio calculations to determine the energetics of the relevant reactant products and intermediates and reaction window calculations to rationalize the state-selectivity of the SET processes.

2. Experimental details

The apparatus employed in this study has been described in detail in previous publications [42] and is illustrated in Fig. 2. Briefly, the apparatus consists of an electron-ionization (150 eV) ion source, in which the desired dications are generated from an appropriate precursor gas (SF_6 in this case). All the ions formed in the source are extracted using ion optics and passed to a velocity filter. The resulting dication beam is re-focussed and decelerated to the chosen collision energy, typically between 4 eV and 16 eV in the laboratory frame. The collision energies

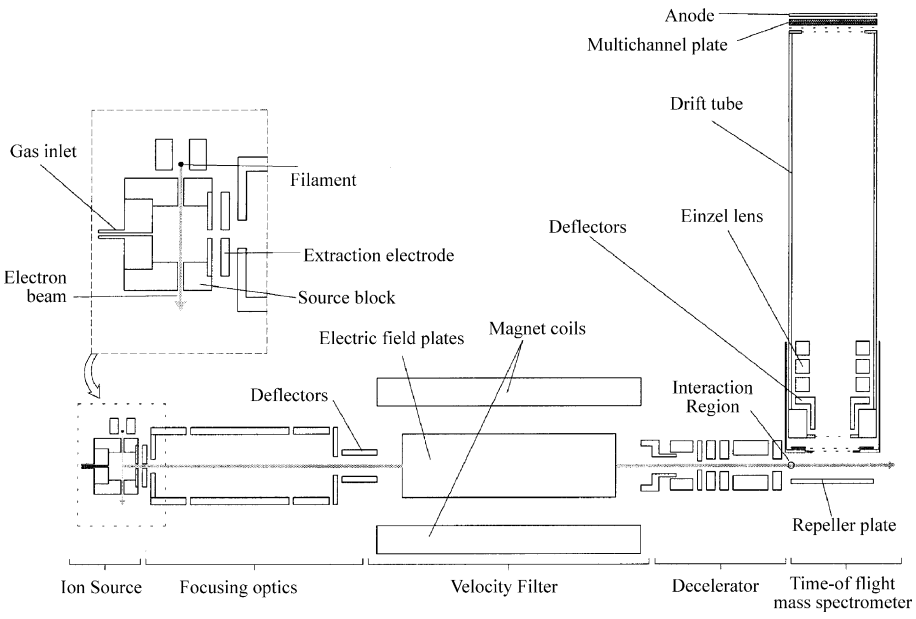

Fig. 2. Schematic diagram of the experimental apparatus.

we employ are relatively low in order to encourage bond-forming reactions. In the experiments reported in this paper, due to the low numbers of SF^{2+} ions generated in the source, a usable dication beam could only be generated at collision energies between 7 eV and 14 eV in the laboratory frame. Following the decelerator, the dication beam encounters a jet of the neutral reactant, Ar in this case, in the source region of a linear time-of-flight mass spectrometer (TOF-MS). The pressure in this collision region is kept low (typically 4×10^{-6} mbar) to ensure single-collision conditions are maintained [43].

Application of a 400 V pulse across the source region of the TOF-MS extracts all the ions present, both products and unreacted dications, into a second accelerating field and subsequently into a drift tube and finally the ions impact on a microchannel plate (MCP) detector. The repeller plate is pulsed at a frequency of 50 kHz, so pulses occur every 20 μs, a period to be compared with typical ionic flight times of less than 6 μs. Each repeller plate pulse is triggered by a pulse generator, which simultaneously starts a multi-hit time-to-digital converter (TDC), commencing the timing cycle. Ion signals from the MCP are amplified, discriminated and passed to the TDC. It is important to note that the discriminator has a dead time of 32 ns following the processing of an ion signal. If two unreacted dications reach the detector following a single pulse of the repeller plate, the mass resolution is such that these ions will arrive within 32 ns of each other and so only one ion will be recorded. These counting losses can become important in extracting cross-sections from our mass spectra as explained in detail below.

3. Data processing

The ionic flight times we record are sent to a PC where they are added to a histogram of ion counts as a function of flight time, a TOF spectrum. A single spectrum is recorded for 5000 cycles, with each cycle involving gathering 512 kb of data. A TOF spectrum typically takes between 30 min and 2 h to collect, depending on the dication beam current. The ionic time of flight spectrum can be readily converted into a mass spectrum using the standard TOF-MS relationship [44]:

$$t = k\sqrt{\frac{m}{z}} + c \tag{12}$$

To use Eq. (12), the constants k and c, which depend on the electric fields in the mass spectrometer and the time delay in the detection electronics, are determined in a calibration experiment.

At least three "datasets" are recorded at each collision energy, each dataset comprising two mass spectra taken with the collision gas absent and a minimum of two mass spectra taken with the collision gas present. All the spectra in a given dataset are scaled so that the unreacted dication peak has the same intensity, and then the *reaction* (neutral gas present) and *background* (neutral gas absent) spectra are separately averaged. Background spectra are taken in order to identify and remove any product ion signals resulting from unimolecular decay of the parent dication or from impurity ions in the dication beam. By comparison of the background and reaction mass spectra, the ion signals corresponding to the bimolecular reactions occurring in the collision system are identified. The magnitude of these product ion signals is then calculated by subtracting, on a peak-by-peak basis, the signal in the averaged background spectrum from the signal of the corresponding peak in the averaged reaction spectrum. Before this subtraction, the contribution of stray ions, which leads to a non-zero baseline in the mass spectra, is also removed. The resulting product signals are then normalized to the signal from the parent dication in the averaged background spectra to give a product ratio R_{obs}. These raw ratios are extracted for each product ion of interest and then corrected for the effect of counting statistics and converted into reaction cross-sections in arbitrary units as described below.

In our experiments the dication current is always kept sufficiently low so that, on average, less than one dication is detected per repeller plate pulse. However, if the average number of dications per pulse approaches unity, it becomes statistically more likely that on some occasions two dications will reach the detector following a single repeller plate pulse [17]. As described above, due to the space-focussing in our TOF-MS, if this situation arises only the first dication of the pair will be counted. Hence, at higher beam currents the parent dication intensity recorded in the mass spectrum will increasingly underestimate the true beam intensity, and so the observed product ratios R_{obs} will overestimate the true product ratios R_{true}. This statistical problem is corrected empirically, as calibration experiments have shown that the following relationship exists between the observed and the true product ratios [17]:

$$\frac{R_{obs}}{R_{true}} = \frac{a}{t^b} + 1 \tag{13}$$

In Eq. (13), t is the time taken to collect the data, which is inversely proportional to the dication beam current given the constraint of a spectrum running for a fixed number of cycles, and a and b are constants. Previous calibration of the instrument has shown that a and b are independent of the collision system [17].

The counting effects, described above, do not affect the collection of product ions, as the product ion intensities are typically more than 1000 times weaker than the parent dication intensity. Thus, the probability of two product ions of the same mass arriving at the detector following the same repeller plate pulse is negligible.

The absolute cross-section for production of an ion is proportional to the flux of that product across the source region of the TOF-MS. However, as will be shown below, determining the constant of proportionality in this relationship and, hence extracting absolute reaction cross-sections from our data is experimentally very difficult. Therefore, as described below, we usually extract integral reaction cross-sections *in arbitrary units* (σ'_j) from our data, these cross-sections being proportional to the absolute reaction cross-sections [17].

The flux of a reaction product, F_j can be related to the flux of incident dications, F_d, by:

$$F_j = \sigma_j N_n L_0 F_d \tag{14}$$

In Eq. (14), N_n is the number density of the neutral collision gas, L_0 is the length over which the dication beam is attenuated by the neutral reactant and σ_j is the absolute reaction cross-section for forming species j.

The intensity I_j of the signal from product species j in the mass spectrum is determined by the number of species j in the region of space in the source region of the TOF-MS that is imaged onto the detector, *not* the flux of products across the source region. To convert our measurements of the ion densities to fluxes, to allow us to extract values of σ'_j, we have to consider the ionic velocities across the source region. As has been discussed before, product ions are formed from a cylindrical dication beam that propagates across the source region of the TOF-MS (Fig. 3). Thus, product ions will be formed in a cylindrical volume V_0 of cross-sectional

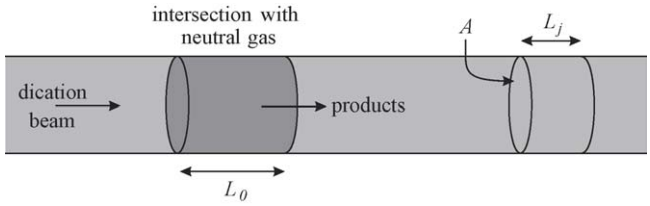

Fig. 3. Diagram illustrating the sampling of the fast forward-scattered products from SET reactions from a volume V_j. The region encompassed by the interaction between the dication beam and the neutral gas is a cylinder of length L_0 and cross-sectional area A.

area A and length L_0 where the dication beam intersects the gas jet. For each product, a length L_j of a further cylindrical volume V_j will be imaged onto the detector (Fig. 4). Note that V_j is the volume in which species j must present, when the repeller plate is pulsed, in order to be detected. Given the relationship between the flux of a species, its density n and its velocity v, we therefore have the following relationship between the mass spectral intensity I and the flux for an arbitrary species moving across the source region of the TOF-MS:

$$I = nV = nLA = \frac{F}{v}LA \tag{15}$$

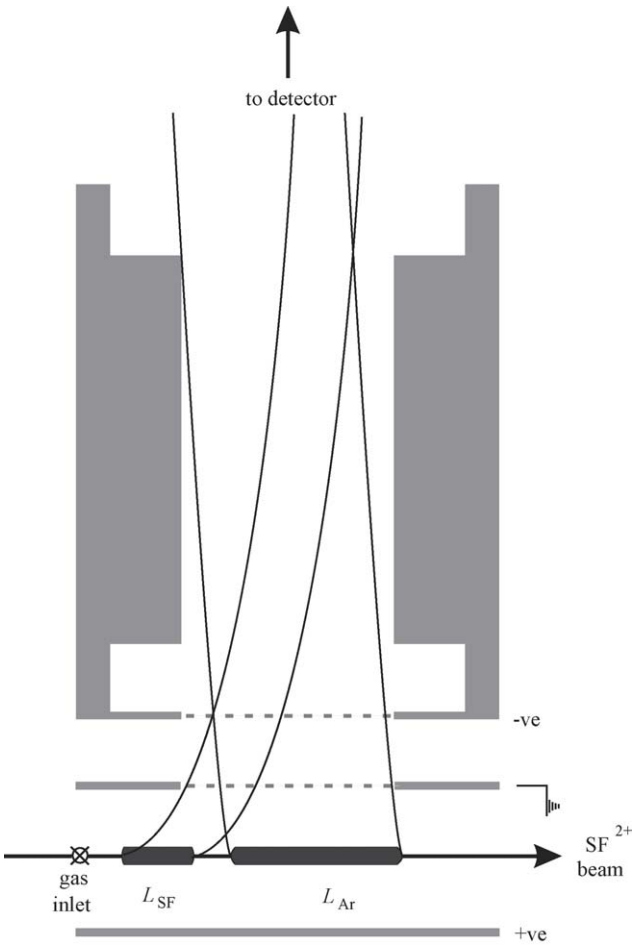

Fig. 4. The length L_j of the ion beam that is imaged onto the detector depends on the velocity of ion j. Fast-moving ions (SF^+, S^+) are sampled from short cylinders early in the source region, whilst slower ions (Ar^+) are sampled from longer cylinders later in the source region.

Using Eq. (15) explicitly to express the fluxes in Eq. (14) for the product species (j) and the dication (d) we have:

$$\frac{I_j v_j}{L_j A_j} = \sigma_j N_n L_0 \frac{I_d v_d}{L_d A_d} \tag{16}$$

For the forward-scattered ions from electron transfer reactions, the cross-sectional area of the ion beam, the neutral gas density and the interaction length are all constants as the mass spectral intensities are recorded in the same experiment. Thus, defining $\sigma'_j = \sigma_j / N_n L_0$ as the absolute cross-section in arbitrary units we have:

$$\sigma'_j = \frac{v_j}{v_d}\frac{L_d}{L_j}\frac{I_j}{I_d} = \frac{v_j}{v_d}\frac{L_d}{L_j} R_{true} \tag{17}$$

The dication velocity (v_d) is known from the beam energy and, as described before, the product velocity can be estimated using momentum and energy arguments [16,17,39–41]. Briefly, to determine the velocity across the source region of the product ion we firstly assume that a typical kinetic energy release of a charge transfer reaction is about 6 eV, as has been determined experimentally [8,10,45]. For a charge transfer reaction, we also know that the reaction dynamics are dominated by forward-scattering [4,13,42]. Thus, given the above kinetic energy release we can estimate the average velocity of the products for such an electron transfer process. Once v_j has been estimated the length of the source region from which these product ions are imaged onto the detector L_j can be calculated from the internal dimensions of the TOF-MS and the applied voltages.

In most instances the above data processing works well, and there is good agreement between the values of σ'_j we derive using this procedure and those of other workers for fast, forward-scattered ions generated in dication SET reactions [39,41,45]. However, problems with the above procedure arise when the laboratory frame velocity of a reaction product is low. Such low laboratory frame velocities are possible if we consider the detection of the backward-scattered products (Ar^+) of an electron transfer reaction. In previous work we have not attempted to quantify the intensities of these slow ions. The low laboratory frame velocities of the Ar^+ product ions arise due to the low experimental centre-of-mass collision energies and the high kinetic energy releases of the dicationic SET reactions. Given these conditions, the Ar^+ ions, which are back-scattered in the centre-of-mass frame, have low velocities across the source region of the TOF-MS or in fact can even be back-scattered in the laboratory frame. For example, in the current collision system, the Ar^+ ions are calculated to have laboratory frame velocities of between 400 m s^{-1} (at a laboratory frame collision energy of 14 eV) and −1000 m s^{-1} (at 6 eV collision energy); far slower than SF^+ ions, which have laboratory frame velocities of 7000 m s^{-1} and 5500 m s^{-1} under the same conditions.

For the slow Ar^+ ions discussed above, Eq. (17) is not applicable. As v_j decreases L_j increases but, for very slow ions, L_j is limited by the internal dimensions of the spectrometer. The shortcomings of Eq. (17) can be explained by considering the quantity L_j/v_j, which can be interpreted as the residence time of a product ion in the cylindrical volume, of length L_j, of the source region that is imaged onto the detector (Fig. 4). As $v_j \to 0$, in the absence of stray fields, the residence time should tend to very large values. However, in practice, due to the pulsed nature of the experiment, the experimental maximum residence time of an ion is limited by the period of the pulsing of the repeller plate. In the current experimental arrangement, a repeller plate pulse occurs every 20 μs with a duration of 10 μs, giving a maximum residence time of an ion in the source of 10 μs. In fact, as the dication beam undoubtedly takes a finite time to re-stabilize after its deflection by the repeller plate pulse, the maximum residence time will be slightly less than 10 μs. Thus, we can rewrite Eq. (17) in terms of the residence time τ of the ion of interest in the volume of the source that is imaged onto the ion detector:

$$\text{if } \tau_j < 10\,\mu s \quad \text{then } \sigma'_j = \frac{\tau_d}{\tau_j} R_{true} \tag{18}$$

$$\text{otherwise } \sigma'_j = \frac{\tau_d}{10} R_{true} \tag{19}$$

Given the above equation we are now, in principle, able to extract values of σ'_j for both the fast forward-scattered ions and the slow backward-scattered ions.

4. Reaction window calculations

As will be discussed in detail below, we observe two SET reactions following collisions of SF^{2+} with Ar. In order to rationalize the relative intensity of these two channels we have performed a calculation of their relative cross-sections using reaction window theory. The methodology for these calculations has been described in detail before [2,46]. Briefly, the probability δ of remaining on a diabatic potential curve through a curve-crossing is a function of the gradients of the two potential curves at the crossing radius, V'_1 and V'_2, the relative radial velocity at the crossing point, $v_r(b)$, and the electronic coupling matrix element, H_{12}.

$$\delta = \exp\left(\frac{-\pi |H_{12}|^2}{2\hbar |V'_1 - V'_2| v_r(b)}\right) \tag{20}$$

As discussed below, the relative radial velocity is a function of the impact parameter b, and the probability P of SET is related to δ by (3); hence, P is also a function of b. The calculated cross-section for electron transfer is then the sum of P over all appropriately weighted values of b for which the collision system reaches the crossing radius.

$$\sigma_{calc} = \int_0^{b_{max}} 2\pi b P(b)\, db \tag{21}$$

As shown in Fig. 1, it is important to realize that there are likely to be several product asymptotes accessible to a SET reaction, these different asymptotes corresponding to different electronic states of the product monocations. If the energies of the accessible electronic states of the product monocations are known then the above numerical methodology can be used to determine the relative reaction cross-section for populating each product asymptote. To do this, as described before [2,46], we calculate the curve-crossing radius for each accessible product asymptote by setting our prototypical reactant (polarization

attraction) and product (Coulombic repulsion) potentials to have an asymptotic energy difference equal to the reaction exothermicity for forming the product asymptote of interest. This procedure requires only the polarizability of the neutral species and the relevant exothermicity. By determining the intersection of the potentials we can calculate the crossing radius, $|V_1' - V_2'|$ and we estimate a value for H_{12} using the semi-empirical formula of Olson et al. [47]. Using the form of the reactant potential, and knowing the collision energy of our experiments, we can then determine b_{max}, the largest impact parameter for which the collision system will reach the crossing radius. We are then in a position to evaluate the integral in Eq. (21), recalling, as noted above, that the radial velocity of the collision system at the crossing is a function of the impact parameter. The evaluation of Eq. (21) gives the cross-section for populating the relevant product asymptote and the procedure is then repeated for the other accessible product asymptotes. As noted above, the various accessible electronic states of the products may be stable, or alternatively may dissociate. For example, in the present experiment S^+ ions are generated by dissociation of SF^+ ions formed in electronically excited states. If we know the fate of the accessible electronic states of the products we can then use our calculations of the cross-sections for populating these electronic states to predict the relative intensities of the various product ions that we observe [1,2,17,36,46,48,49].

5. Results

Mass spectra were recorded, as described above, at collision energies from 6.0 eV to 14.0 eV in the laboratory frame corresponding to 2.6–6.2 eV in the centre-of-mass frame. Comparison of the reaction and background mass spectra (Fig. 5) clearly indicates the formation of S^+, SF^+, Ar^+ and ArS^{2+} ions. We do not detect the formation of F^+ from bimolecular collisions. The absence of F^+ signals following bimolecular reactions has also been reported following collisions of other fluorinated dications [1,26,48,50]. We also do not observe any Ar^{2+} ions, which would be produced by double electron transfer processes. Given the absence of any F^+ signals it is clear that two SET reactions are occurring in the SF^{2+} + Ar collision system together with a bond-forming reaction generating ArS^{2+}:

$$SF^{2+} + Ar \rightarrow SF^+ + Ar^+ \quad (22)$$

$$SF^{2+} + Ar \rightarrow S^+ + F + Ar^+ \quad (23)$$

$$SF^{2+} + Ar \rightarrow ArS^{2+} + F \quad (24)$$

For the products of the SET reactions the relevant ion intensities in the mass spectra were processed, as also described above, to yield the relevant σ_j' values for these ions as a function of collision energy. Note that for the formation of the S^+ ion we assume, as has been determined experimentally for similar collision systems [26], that the energy release upon dissociation of the excited electronic states of SF^+ to from S^+ is negligible in comparison to the energy release involved in the separation of the SF^+ and Ar^+. Thus, the S^+ ion moves across the source region of our experiment with approximately the velocity of the parent SF^+ ion. We discuss the extraction of the σ_j' values for the formation of the ArS^{2+} ion in more detail below.

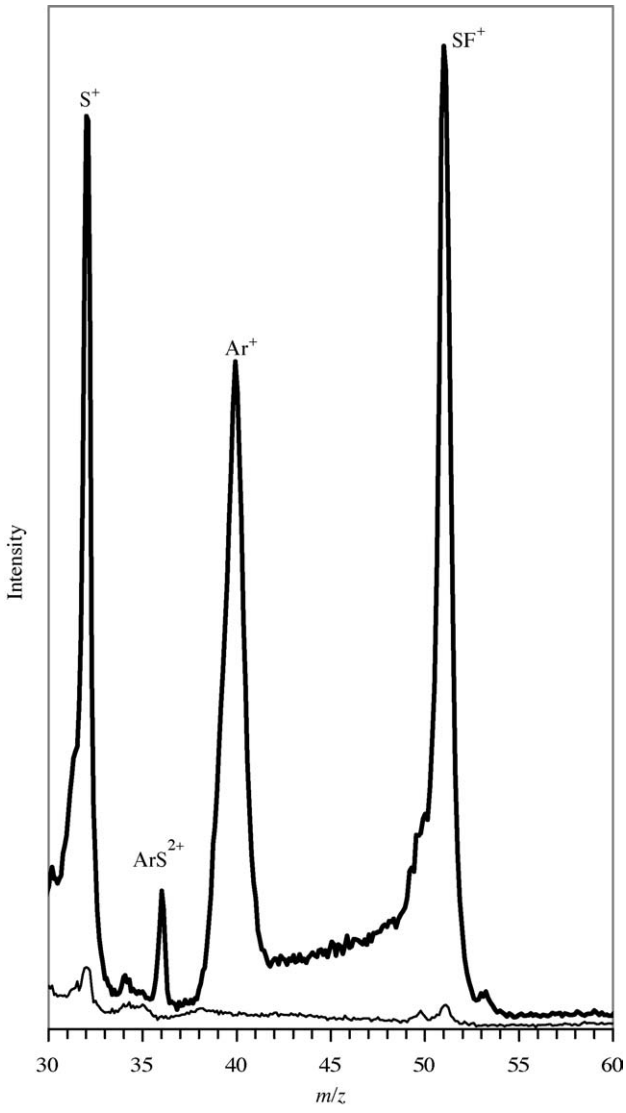

Fig. 5. An example mass spectrum for SF^{2+} + Ar. The thick line indicates a spectrum recorded with the collision gas (Ar) present, whilst the thin line indicates an appropriately normalized spectrum recorded with the collision gas absent.

6. Discussion

6.1. Electron transfer reactions

Fig. 6 shows the values of σ_j' we derive for the formation of SF^+ and S^+ as a function of centre-of-mass frame collision energy. Note that the ratio between the σ_j' values for forming SF^+ and S^+ is approximately 2:1. The values of σ_j' do not vary significantly with collision energy over the range of our experimental investigations. A similar insensitivity to the collision energy has been observed for several other SET reaction of dications in this energy regime [50]. To perform the Landau–Zener calculations outlined above, to attempt to account for the relative intensities

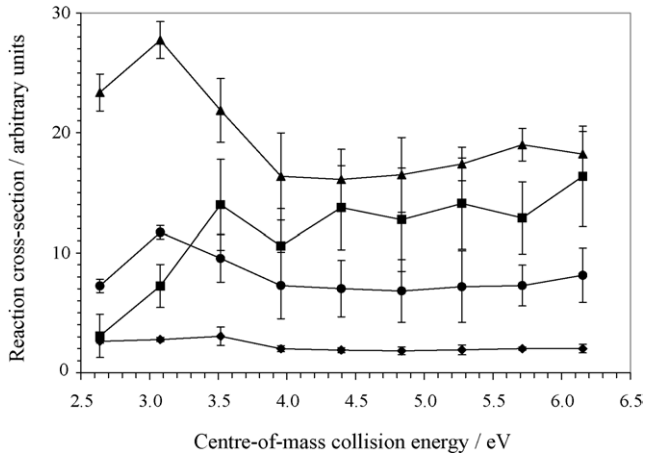

Fig. 6. Absolute reaction cross-sections σ'_j, in arbitrary units, for the formation of SF^+ (▲), S^+ (●), Ar^+ (♦) and $ArS^{2+} \times 100$ (■) as a function of centre-of-mass frame collision energy.

of SF^+ and S^+ that we observe, requires the relative energies of the relevant electronic states of SF^{2+} and SF^+. Little experimental information is available on the relative energetics of the monocationic and dicationic states of SF^+. Hence, we have determined these energies using a quantum chemical approach. The detailed results of these quantum chemical investigations into the potential energy curves of SF^{2+} and SF^+ will be reported in detail elsewhere [51,52]. Briefly, the computational modelling involved generating potential energy curves for electronic states of SF^+ and SF^{2+} by performing single-point energy calculations at 0.05 Å intervals using the state-averaged AQCC method with a full valence active space, coupled with an uncontracted basis set as implemented in Molpro v.2002.3 consisting of 16s11p3d2f1g functions for S atoms and 12s6p3d2f1g functions for F atoms [53]. The results from the computational work show that the ground dication state of SF^{2+} ($X\ ^2\Pi$) is metastable, as it possesses a significant barrier (~4.5 eV) to charge separation. The first SF^{2+} excited state ($A\ ^2\Pi$) is also metastable, possessing a barrier of ~2.5 eV to charge separation, and lies 4.0 eV above the ground state. A further six metastable dication states lie within 6.0 eV of the ground state, but these are all much more weakly bound (<1 eV). Thus we may expect our dication beam to be predominantly composed of SF^{2+} ions in both their ground and first excited electronic states. With regard to the monocation we find that the first three electronic states of SF^+ ($X\ ^3\Sigma^-$, $a\ ^1\Delta$, $b\ ^1\Sigma^+$) are bound; the first dissociative state ($A\ ^3\Pi$) lies 5.7 eV above the ground state of SF^+ and the higher electronic states of SF^+ we calculate are also dissociative [51,52]. The adiabatic ionization energy of SF^+ is calculated to be 21.3 eV and the first ionization energy of SF is experimentally established as 10.1 eV [54], a value in good agreement with our calculations [51,52]. The ionization energy for populating the $3p^{-1}$ (^2P) electronic state of Ar^+ is well known, and hence we are able to evaluate the exothermicities for populating the accessible $SF^+ + Ar^+$ product asymptotes, which are listed in Table 1. Note that SET reactions involving the population of higher electronic states of Ar^+, for example the $3s^{-1}(^2S_{1/2})$ state, are endothermic and thus are not expected to be populated in Landau–Zener style transitions, as has been confirmed experimentally for other collision systems [54].

Table 1
Landau–Zener calculations showing relative SET cross-sections σ_{SET} (in Å^2) and exothermicities ΔH from the ground (X) and first excited states (A) of SF^{2+} to the first six electronic states of SF

Electronic state of SF^+ product	Electronic state of SF^{2+} reactant			
	$X\ ^2\Pi$		$A\ ^2\Pi$	
	ΔH (eV)	σ_{SET}	ΔH (eV)	σ_{SET}
$X\ ^3\Sigma^-$ ($\rightarrow SF^+$)	−5.5	1	−9.5	0
$a\ ^1\Delta$ ($\rightarrow SF^+$)	−4.4	12	−8.4	0
$b\ ^1\Sigma^+$ ($\rightarrow SF^+$)	−3.5	21	−7.5	0
$A\ ^3\Pi$ ($\rightarrow S^+ + F$)	+0.3	0	−3.7	23
$d\ ^1\Pi$ ($\rightarrow S^+ + F$)	+1.4	0	−2.7	3
$D\ ^3\Pi$ ($\rightarrow S^+ + F$)	+2.2	0	−1.9	0

These calculations were performed for a collision energy of 10.0 eV in the laboratory frame, equivalent to 4.4 eV in the centre-of-mass frame.

Table 1 shows SET cross-sections we calculate for populating the various electronic states of SF^+, formed together with $Ar^+(^2P)$, from the two electronic metastable states of SF^{2+}. It can be seen from Table 1 that the probability of the SET reaction populating the dissociative electronic states of SF^+ is negligible if the SF^{2+} is not electronically excited. This implies that the S^+ signal observed in the mass spectra must result from the population of the dissociative higher lying states of SF^+ by the SET reactions of the first excited state of SF^{2+}, supporting our expectation that our dication beam is composed of SF^{2+} ions in both their ground and first excited states. Hence, the Landau–Zener calculations indicate that the magnitude of the S^+ signal we observe is a measure of the relative population of the ground and first excited electronic states of SF^{2+} in our beam. Given the cross-sections listed in Table 1, and our experimentally observed ratio of S^+ to SF^+, we can see that there must be a significant population of the $SF^{2+}(A)$ state in our beam. We estimate that the beam comprises approximately half as many dications in the first excited electronic state as dications in the ground electronic state.

The value of σ' for the formation of Ar^+ from the $SF^{2+} + Ar$ collision system should, of course, be equal to the sum of the σ' values for the formation of SF^+ and S^+ since Ar^+ must be produced in all SET reactions. However, as shown in Fig. 6, the value of σ' we determined from our data for the formation of Ar^+ is significantly lower than this value. This discrepancy arises due to the values of the constants involved in the "arbitrary units" in which we express our values of σ'_j. For example, Eq. (16) shows that the constant of proportionality between our derived σ'_j values and the true absolute cross-sections depends on the number density of the neutral gas. Fig. 4 shows that the Ar^+ ions, being backward-scattered in the centre-of-mass frame, are sampled from a spatially distinct portion of the source region to the forward-scattered product ions. Thus, the arbitrary units for our values of σ'_j for the "fast" product ions are different to the arbitrary units for the values of σ' for forming Ar^+ because of the different number density of Ar in the spatially distinct regions in which the relevant ions are formed. The neutral gas jet is

positioned above the ion beam, before the source region of the TOF-MS (as shown in Fig. 4). This position is ideal for the generation and collection of fast product ions from SET reactions. However, since the Ar^+ ions are so slow in the laboratory frame the Ar number density will be substantially lower in the region from which Ar^+ ions are formed compared with that for the SF^+ and S^+ ions. Thus, given our current experimental arrangement we cannot expect the σ'_j values we derive to be comparable for the "fast" and "slow" product ions. In principle, one could overcome this problem by introducing the target gas effusively well away from the source region of the TOF-MS so that the neutral gas density will be uniform across the interaction region, although this would present problems with attenuation of the dication beam before it reaches the TOF-MS. However, despite the above problems it is satisfying to see that (Fig. 6) the energy dependence of the σ' values for forming Ar^+ is effectively identical to that we observe for S^+ and SF^+ as one would expect. Thus, whilst not being able to extract directly comparable σ' values for the slow backward-scattered ions from SET reaction, we now can at least determine the collision energy dependence of their reaction cross-sections. A significant step forward in the data we can extract from our experiments.

6.2. Formation of ArS^{2+}

As discussed above, the peak we observe in the in the mass spectrum at $m/z = 36$ (Fig. 5) is assigned to ArS^{2+}, clearly indicating the occurrence of reaction (24). Fig. 6 shows the values of σ' for the formation of ArS^{2+} as a function of collision energy. As shown below, the formation of ArS^{2+} is thought to proceed via the formation of an $ArSF^{2+}$ collision complex. Hence, the extraction of the σ' values for ArS^{2+} assumes that the kinetic energy release accompanying the dissociation of the collision complex is negligible and the laboratory frame velocity of ArS^{2+} is assumed to be equal to the velocity of the centre-of-mass of the collision system. It appears clear from Fig. 6 that the cross-section for this bond forming reaction rises from a threshold just below 2.5 eV. A more accurate determination of this threshold is not possible in our experiments due to the small ArS^{2+} signal and the low flux of SF^{2+} in these experiments. Note that in Fig. 6 the σ' values for forming ArS^{2+} are multiplied by a factor of 100.

As discussed above, the observation of a doubly charged molecular product form the reaction of a small molecular dication with a rare gas atom is rather unusual. A schematic model proposed to rationalize the occurrence of bond-forming dicationic reactions has been presented before [4,8,10], and is illustrated in Fig. 7. The left hand side diagram represents the approach of the reactant dication and the neutral. However, for the reactants to achieve the intimate contact they require to form new chemical bonds, the collision system must successfully pass through the curve-crossing in the entrance channel that leads to SET (Point 1, Fig. 7). If the collision system passes through Point 1 then a collision complex can be formed and the necessary chemistry may occur. As the products separate they must pass through the curve-crossing at Point 2 (Fig. 7), where a change of potential surfaces will result in the formation of a pair of monocations. Indeed, bond-forming reactions forming pairs

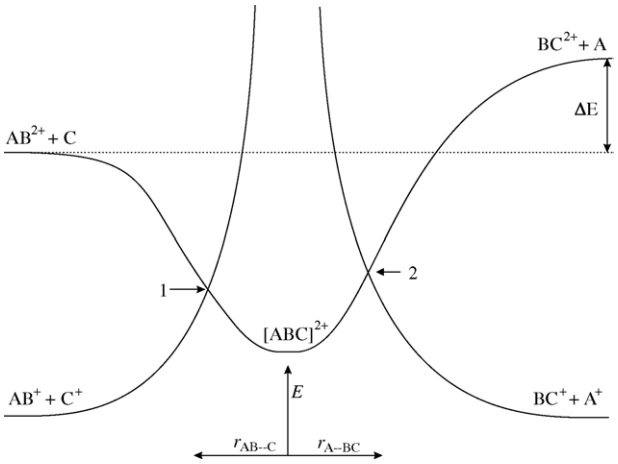

Fig. 7. Schematic potentials showing the route from $AB^{2+} + C$ to $AC^{2+} + B$ [4]. The reactants must avoid switching potential surfaces at Points 1 and 2 and have sufficient kinetic energy to reach the product asymptote (ΔE).

of monocations are often observed following collisions of dications with neutrals [31]. Even if the collision system successfully negotiates this second region of curve crossings it must possess sufficient kinetic energy ΔE to reach the asymptotic limit corresponding to $ArS^{2+} + F$. Of course, in addition to these energetic and dynamic considerations, the doubly charged product must be formed in a non-dissociative state in order to be detected.

Fig. 8 shows the relative energetics of the various critical points in the reaction mechanism forming ArS^{2+} for our collision system. All of the product asymptotes in Fig. 8 can be reached in a spin allowed fashion from the ground state of SF^{2+} and, hence, other factors must account for the propensity for forming ArS^{2+} in this collision system. To derive some of the energetics shown in Fig. 8, we have performed quantum chemical calculations to determine the energies and geometries of species containing an

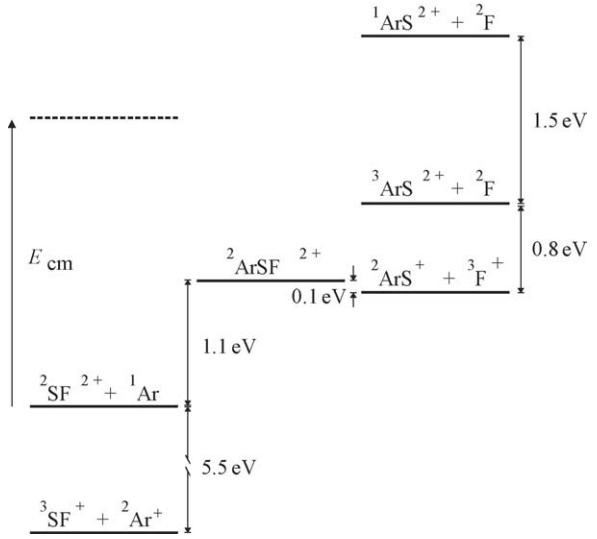

Fig. 8. Relative energies of the reactant and product asymptotes associated with the formation of ArS^{2+} from the reaction of $SF^{2+} + Ar$. See text for details. E_{cm} indicates the minimum collision energy available in the experiments reported in this paper.

Table 2
Optimised geometries calculated for relevant species containing an Ar—S bond

	r(Ar—S) (Å)	r(F—S) (Å)	∠(Ar—S—F)
$^2ArSF^{2+}$	2.14	2.05	167.47°
$^2ArS^+$	2.13	–	–
$^3ArS^{2+}$	2.06	–	–
$^1ArS^{2+}$	2.02	–	–

Ar–S bond. These calculations were performed using Gaussian 98 [55] implemented on a Linux workstation. Optimised geometries (see Table 2) were determined using an MP2 algorithm with a cc-VQZ basis set and the energies of these geometries (relative to $Ar^+ + F^+ + S$) were then evaluated using a coupled cluster [CCSD(T)] algorithm. As described above, the ionization energy of SF^+ was calculated via an alternative methodology as part of a different investigation [51,52]. However, since the ionization energy and heat of formation of SF are known experimentally [54], the relative energy of the reactant asymptote can be located appropriately, as is shown in Fig. 8.

In the present experiment the collision system readily crosses at the first curve intersection, (Point 1, Fig. 7) as strong signals of SF^+ (and S^+) and Ar^+ are observed. However, the observation of products with new chemical bonds shows that a significant number of collisions do not cross at this first intersection. For the equilibrium geometries of ArS^{2+} and ArS^+, the asymptote corresponding to $ArS^+ + F^+$ lies just 0.8 eV below the asymptote corresponding to $^3ArS^{2+} + F$ and 2.3 eV below that corresponding to $^1ArS^{2+} + F$ (Fig. 8). These small energy differences between these asymptotes means that the critical curve-crossings in the exit channel, towards $ArS^{2+} + F$ (Point 2, Fig. 7), occur at large interspecies separations. Hence, the probability of crossing at Point 2 (Fig. 7) will be small. This energetic argument clearly explains why no ArS^+ signal is observed in this collision system, even though the observation of ArS^{2+} tells us there will be a product flux through the intersections in the exit channel. Note that our energetics (Fig. 8) show that excited singlet state of ArS^{2+} lies 1.5 eV above the ground triplet state of this dication and that accessing these asymptotes from the ground state reactants requires the centre-of-mass kinetic energy to exceed 1.8 eV and 3.6 eV, respectively. The lower of these thresholds is below our experimental collision energy range. However, from Fig. 6 the values of σ' for forming ArS^{2+} appear to be falling towards a threshold at approximately 2 eV, in accord with the threshold expected from our calculations of the energetics. In addition there appears to be a sharp increase in the σ' values for forming ArS^{2+} close to the 3.6 eV collision energy calculated to be required to open the channel generating $^1ArS^{2+}$. Thus, our experimental data indicates that perhaps both the singlet and triplet states of the dicationic product are populated in this reaction. The contribution of excited SF^{2+} reactant ions to the reaction cannot be confidently ascertained from this data.

It is likely that at higher collision energies than are reported in this paper, the cross-section for forming ArS^{2+} will begin to fall off, as has been observed for the formation of ArC^{2+} [6,11]. This fall in the cross section results as the increase in the internal energy of the collision system results in the population of dissociative excited states of the product dication.

7. Conclusions

The formation of S^+ and SF^+ in SET reactions between SF^{2+} and Ar has been detected and the cross-sections, in arbitrary units, for forming these species have been evaluated as a function of collision energy from 2.6 eV to 6.2 eV in the centre-of-mass frame. The form of this SET reactivity has been rationalized by Landau–Zener calculations, which indicate that the S^+ product results from the dissociation of excited electronic states of SF^+ populated by the reaction of the first excited electronic state of SF^{2+}. The calculations also indicate the stable SF^+ ions detected result from the SET reactions of the ground state of SF^{2+}. The reactivity of this collision system also involves an unusual bond-forming reaction, which generates ArS^{2+}. Quantum chemical calculations of the relevant energetics show that the lowest lying singlet and triplet states of ArS^{2+} are bound and are energetically accessible for this collision system at the above collision energies. The observation of ArS^{2+} has been rationalized in terms of the relative energetics of the competing chemical and electron transfer reactions. This analysis shows that electron transfer in the exit channel between the separating ArS^{2+} and F atom is likely to be inefficient, explaining why we detect the observed products and not a pair of monocations.

Acknowledgements

The authors acknowledge the financial support of the EPSRC, the EU (RTN1-2000-00025) and the Leverhulme Trust for these experiments. PWB also acknowledges the support of the EPSRC via a DTA studentship. The authors are also grateful for helpful discussions on theoretical methodology with Nik Kaltsoyannis and Natalie Lambert. We also gratefully acknowledge the members of the EU MCInet network for helpful discussions.

References

[1] M. Manning, S.D. Price, S.R. Leone, J. Chem. Phys. 99 (1993) 8695.
[2] S.A. Rogers, S.D. Price, S.R. Leone, J. Chem. Phys. 98 (1993) 280.
[3] S.D. Price, M. Manning, S.R. Leone, J. Am. Chem. Soc. 116 (1994) 8673.
[4] Z. Herman, Int. Rev. Phys. Chem. 15 (1996) 299.
[5] A. Ehbrecht, N. Mustafa, C. Ottinger, Z. Herman, J. Chem. Phys. 105 (1996) 9833.
[6] P. Tosi, W.Y. Lu, R. Correale, D. Bassi, Chem. Phys. Lett. 310 (1999) 180.
[7] P. Tosi, R. Correale, W.Y. Lu, S. Falcinelli, D. Bassi, Phys. Rev. Lett. 82 (1999) 450.
[8] Z. Herman, J. Zabka, Z. Dolejsek, M. Farnik, Int. J. Mass Spectrom. 192 (1999) 191.
[9] D. Schroder, H. Schwarz, J. Phys. Chem. A 103 (1999) 7385.
[10] L. Mrazek, J. Zabka, Z. Dolejsek, J. Hrusak, Z. Herman, J. Phys. Chem. A 104 (2000) 7294.
[11] W.Y. Lu, P. Tosi, D. Bassi, J. Chem. Phys. 112 (2000) 4648.
[12] O. Witasse, O. Dutuit, J. Lilensten, R. Thissen, J. Zabka, C. Alcaraz, P.L. Blelly, S.W. Bougher, S. Engel, L.H. Andersen, K. Seiersen, Geophys. Res. Lett. 29 (2002) (Art No. 1263).
[13] S.M. Harper, W.-P. Hu, S.D. Price, J. Phys. B. 35 (2002) 4409.

[14] J. Roithova, R. Thissen, J. Zabka, P. Franceschi, O. Dutuit, Z. Herman, Int. J. Mass Spectrom. 228 (2003) 487.
[15] J. Roithova, J. Zabka, J. Hrusak, R. Thissen, Z. Herman, J. Phys. Chem. A 107 (2003) 7347.
[16] N. Tafadar, S.D. Price, Int. J. Mass Spectrom. 223–224 (2003) 547.
[17] D. Kearney, S.D. Price, Phys. Chem. Chem. Phys. 5 (2003) 1575.
[18] D. Ascenzi, P. Franceschi, P. Tosi, D. Bassi, M. Kaczorowska, J.N. Harvey, J. Chem. Phys. 118 (2003) 2159.
[19] N. Lambert, D. Kearney, N. Kaltsoyannis, S.D. Price, J. Am. Chem. Soc. 126 (2004) 3658.
[20] S.M. Harper, W.-P. Hu, S.D. Price, J. Chem. Phys. 120 (2004) 7245.
[21] S.M. Harper, W.-P. Hu, S.D. Price, J. Chem. Phys. 121 (2004) 3507.
[22] J. Roithova, D. Schroder, H. Schwarz, Chem. A Eur. J. 11 (2005) 628.
[23] J. Roithova, D. Schroder, J. Loos, H. Schwarz, H.C. Jankowiak, R. Berger, R. Thissen, O. Dutuit, J. Chem. Phys. 122 (2005).
[24] C. Ricketts, W.-P. Hu, S.D. Price, J. Chem. Phys. 123 (2005) (Art No. 134322).
[25] N. Lambert, N. Kaltsoyannis, S.D. Price, J. Zabka, Z. Herman, J. Phys. Chem. A (2005), doi:10.1021/jp052981d.
[26] W.-P. Hu, S.M. Harper, S.D. Price, Mol. Phys. 103 (2005) 1809.
[27] O. Abu-Haija, E.Y. Kamber, D. Mathur, Chem. Phys. Lett. 408 (2005) 5.
[28] T.A. Field, J.H.D. Eland, Int. J. Mass Spectrom. 192 (1999) 281.
[29] S. Hsieh, J.H.D. Eland, Int. J. Mass Spectrom. 167 (1997) 415.
[30] L.H. Andersen, J.H. Posthumus, O. Vahtras, H. Agren, N. Elander, A. Nunez, A. Scrinzi, M. Natiello, M. Larsson, Phys. Rev. Lett. 71 (1993) 1812.
[31] S.D. Price, Phys. Chem. Chem. Phys. 5 (2003) 1717.
[32] D. Mathur, Phys. Rep. 391 (2004) 1.
[33] L.D. Landau, Phys. Z. Sowjetunion 2 (1932) 46.
[34] C. Zener, Proc. R. Soc. Lond. Ser. A 137 (1932) 696.
[35] O. Hadjar, D. Ascenzi, D. Bassi, P. Franceschi, M. Sabidò, P. Tosi, Chem. Phys. Lett. 400 (2004) 476.
[36] S.D. Price, M. Manning, S.R. Leone, Chem. Phys. Lett. 214 (1993) 553.
[37] X.D. Zhou, A.K. Shukla, R.E. Tosh, J.H. Futrell, Int. J. Mass Spectrom. Ion Process. 160 (1997) 49.
[38] B.K. Chatterjee, R. Johnsen, J. Chem. Phys. 93 (1989) 5681.
[39] N. Tafadar, D. Kearney, S.D. Price, J. Chem. Phys. 115 (2001) 8819.
[40] K.A. Newson, S.D. Price, Chem. Phys. Lett. 294 (1998) 223.
[41] K.A. Newson, S.D. Price, Chem. Phys. Lett. 269 (1997) 93.
[42] S.D. Price, J. Chem. Soc. Faraday Trans. 93 (1997) 2451.
[43] K. Yamasaki, S.R. Leone, J. Chem. Phys. 90 (1989) 964.
[44] W.C. Wiley, I.H. McLaren, Rev. Sci. Inst. 26 (1955) 1150.
[45] Z. Dolejsek, M. Farnik, Z. Herman, Chem. Phys. Lett. 235 (1995) 99.
[46] S.D. Price, S.A. Rogers, S.R. Leone, J. Chem. Phys. 98 (1993) 9455.
[47] R.E. Olson, F.T. Smith, E. Bauer, App. Opt. 10 (1971) 1848.
[48] P.H. Champkin, N. Kaltsoyannis, S.D. Price, Int. J. Mass Spectrom. Ion Process. 172 (1998) 57.
[49] Y.Y. Lee, S.R. Leone, P.H. Champkin, N. Kaltsoyannis, S.D. Price, J. Chem. Phys. 106 (1997) 7981.
[50] N. Tafadar, N. Kaltsoyannis, S.D. Price, Int. J. Mass Spectrom. 192 (1999) 205.
[51] N. Lambert, N. Kaltsoyannis, S.D. Price, in preparation.
[52] N. Lambert, Ph.D. Thesis, UCL, 2005.
[53] Molpro is a Package of Ab Initio Programs written by H.J. Werner and P.J. Knowles, with Contributions from R.D. Amos, A. Bernhardsson, A. Berning, P. Celani, D.L. Cooper, M.J.O. Deegan, A.J. Dobbyn, F. Eckert, C. Hampel, G. Hetzer, T. Korona, R. Lindh, A.W. Lloyd, S.J. McNicholas, F.R. Manby, W. Meyer, M.E. Mura, A. Nicklass, P. Palmieri, R. Pitzer, G. Rauhut, M. Sch'utz, H. Stoll, A.J. Stone, R. Tarroni, T. Thorsteinsson.
[54] S. Lias, in: P. Linstrom (ed.), NIST Chemistry WebBook, NIST Standard Reference Database Number 69, National Institute of Standards and Technology, Gaithersburg, MD, 2000, 20899 (http://webbook.nist.gov).
[55] M.J. Frisch, G.W. Trucks, H.B. Schlegel, G.E. Scuseria, M.A. Robb, J.R. Cheeseman, V.G. Zakrzewski, J.A. Montgomery Jr., R.E. Stratmann, J.C. Burant, S. Dapprich, J.M. Millam, A.D. Daniels, K.N. Kudin, M.C. Strain, O. Farkas, J. Tomasi, V. Barone, M. Cossi, R. Cammi, B. Mennucci, C. Pomelli, C. Adamo, S. Clifford, J. Ochterski, G.A. Petersson, P.Y. Ayala, Q. Cui, K. Morokuma, M.D. K., A.D. Rabuck, K. Raghavachari, J.B. Forseman, J. Cioslowki, J.V. Ortiz, B.B. Stefanov, G. Liu, A. Liashenko, P. Piskorz, I. Komaromi, R. Gomperts, R.L. Martin, D.J. Fox, T. Keith, M.A. Al-Laham, C.Y. Peng, A. Nanayakkara, C. Gonzalez, M. Challacombe, P.M.W. Gill, B. Johnson, W. Chen, M.W. Wong, J.L. Andreas, M. Head-Gordon, E.S. Replogle, J.A. Pople, Gaussian 98, Revision A.3, Gaussian, Inc., Pittsburgh PA, 1998.